The Response of the Indian Ocean Dipole Asymmetry to Anthropogenic Aerosols and Greenhouse Gases

TIM COWAN, WENJU CAI, AND BENJAMIN NG

CSIRO Marine and Atmospheric Research, Aspendale, Victoria, Australia

MATTHEW ENGLAND

Climate Change Research Centre, University of New South Wales, Sydney, New South Wales, Australia

(Manuscript received 26 September 2014, in final form 2 December 2014)

ABSTRACT

The tropical Indian Ocean has experienced a faster warming rate in the west than in the east over the twentieth century. The warming pattern resembles a positive Indian Ocean dipole (IOD) that is well captured by climate models from phase 5 of the Coupled Model Intercomparison Project (CMIP5), forced with the two main anthropogenic forcings, long-lived greenhouse gases (GHGs), and aerosols. However, much less is known about how GHGs and aerosols influence the IOD asymmetry, including the negative sea surface temperature (SST) skewness in the east IOD pole (IODE). Here, it is shown that the IODE SST negative skewness is more enhanced by aerosols than by GHGs using single-factor forcing experiments from 10 CMIP5 models. Aerosols induce a greater mean zonal thermocline gradient along the tropical Indian Ocean than that forced by GHGs, whereby the thermocline is deeper in the east relative to the west. This generates strong asymmetry in the SST response to thermocline anomalies between warm and cool IODE phases in the aerosol-only experiments, enhancing the negative IODE SST skewness. Other feedback processes involving zonal wind, precipitation, and evaporation cannot solely explain the enhanced SST skewness by aerosols. An interexperiment comparison in one model with strong skewness confirms that the mean zonal thermocline gradient across the Indian Ocean determines the magnitude of the SST–thermocline asymmetry, which in turn controls the SST skewness strength. The findings suggest that as aerosol emissions decline and GHGs increase, this will likely contribute to a future weakening of the IODE SST skewness.

1. Introduction

The surface warming in the tropical Indian Ocean over the late twentieth century resembles that during the positive phase of the Indian Ocean dipole (IOD), with anomalous cooling in the east IOD pole (IODE; 10°S–0°, 90°–110°E) near Sumatra–Java, and anomalous warming in the west IOD pole (IODW; 10°S–10°N, 50°–70°E). The IOD predominantly develops in the austral winter and peaks in spring (Saji et al. 1999), and, when positive, is associated with anomalously high rainfall across eastern Africa (Behera et al. 2005) and India (Yadav 2013), but drier conditions in Indonesia and southern Australia (Ummenhofer et al. 2009; Cai et al. 2012). Recent studies have used climate model evidence to show that greenhouse gases (GHGs) are the most likely cause of the late-twentieth-century positive IOD-like trend (Dong and Zhou 2014; Cai et al. 2013). In contrast, anthropogenic aerosols have been shown to induce a slowdown in the rate of twentieth-century warming across the tropical Indian Ocean, resembling a negative IOD-like pattern (Dong and Zhou 2014). Further cooling of the subsurface subtropical Indian Ocean has also been attributed to an aerosol forcing (Cowan et al. 2013; Cai et al. 2007), as well as changes in the Southern Hemisphere subtropical jet and tropical precipitation (Rotstayn et al. 2013, 2012). New modeling evidence also suggests that aerosols modify decadal sea surface temperature (SST) variability in the Pacific Ocean, which in turn influences the tropical expansion rate (Allen et al. 2014).

A well-known feature of the IODE region is the negative SST skewness during the austral spring

Corresponding author address: Tim Cowan, CSIRO Oceans and Atmosphere Flagship, 107-121 Station St., Aspendale VIC 3195, Australia.
E-mail: Tim.Cowan@csiro.au

DOI: 10.1175/JCLI-D-14-00661.1

[September–November (SON)] season (Hong and Li 2010; Cai and Qiu 2013). During positive IOD events, cool IODE SST anomalies (SSTAs) tend to grow larger in amplitude than warm SSTAs during negative IOD events (Hong et al. 2008a,b; Cai and Qiu 2013), meaning the IOD is positively skewed (i.e., IOD is defined as IODW minus IODE). Skewness is a measure of the asymmetry of a probability distribution function (Hong et al. 2008a).[1] Observations suggest that the positive IOD skewness merely reflects the negative SST skewness in the IODE region, as the IODW region exhibits only a weak positive SST skewness (Hong et al. 2008a). The IODE SST negative skewness is well captured by climate models that include all radiative forcing agents (Ng et al. 2014b; Ogata et al. 2013; Zheng et al. 2013, 2010). Climate models from phase 5 of the the Coupled Model Intercomparison Project (CMIP5) show that the negative IODE SST skewness will weaken in the twenty-first century as a result of a shoaling thermocline trend (Cai et al. 2013).

One important contributor to the IOD skewness is an asymmetry in the Bjerknes feedback. A description of this feedback is as follows: during positive IOD events, easterly anomalies generate a near-surface Kelvin wave that propagates eastward, upwelling water in the Sumatra–Java region, shoaling the IODE thermocline that further cools the IODE SSTs. In turn, cooler SSTAs enhance the zonal SST gradient across the tropical Indian Ocean, which reinforces the easterly anomalies, completing the Bjerknes feedback. This feedback is an important factor in the simulated strength of the IOD in models from phase 3 of CMIP (CMIP3) and CMIP5 (Liu et al. 2011, 2014), despite doubts raised about the role of the SST–thermocline response in ocean reanalysis products (Hong and Li 2010). The Bjerknes feedback is important in the IODE region, as confirmed in three CMIP5 models, whereby GHGs (aerosols) force an increase in the anomalous easterlies (westerlies) and reduce (enhance) precipitation over the IODE region (Xie et al. 2013). Asymmetry in the SST–thermocline relationship arises because the observed mean thermocline in the IODE region is deep (Cai and Cowan 2013), such that an anomalous deepening produces a surface warming that is far weaker than a surface cooling from an anomalous shoaling (Hong et al. 2008a). If the thermocline gradually shallows, as projected by CMIP5 models, the asymmetry of the SST–thermocline response between the IOD phases should diminish (Cai et al. 2013; Ng et al. 2014b). This is despite CMIP5 models simulating shallower (deeper) IODE (IODW) thermoclines than in observations, meaning the zonal thermocline gradients are positively biased (Cai and Cowan 2013).

Precipitation also plays a role in generating IOD skewness through the negative SST–cloud–radiation feedback (Ng et al. 2014a; Hong et al. 2008a; Hong and Li 2010), whereby warm IODE SSTAs promote increased convection, cloud cover, and precipitation, which effectively damp the SSTAs. If the SSTAs are sufficiently cold, convection can be completely suppressed, leading to cloud-free conditions. This caps the amount of incoming shortwave radiation that reaches the surface of the eastern Indian Ocean, thus allowing for cool SSTAs to grow with no further damping (Hong et al. 2008a). CMIP5 models with a stronger damping (i.e., feedback coefficients that are more negative) tend to generate larger IOD amplitudes (Liu et al. 2014). Global warming is likely to lead to increased asymmetry in the SST–cloud–radiation feedback because of reduced precipitation in the mean climate (Ng et al. 2014a; Cai et al. 2013). Despite this, the IODE SST asymmetry and skewness are projected to weaken in the future, given the shoaling mean thermocline (Ng et al. 2014b).

Other important processes in the tropical Indian Ocean are wind–evaporation–SST feedback and nonlinear dynamic heating. Evaporation can be enhanced if wind speeds are strong enough under cool IODE conditions; however, cool SSTAs can also reduce evaporation depending on the humidity (Ng et al. 2014a). The nonlinear dynamic heating process describes the anomalous advection of anomalous zonal, meridional, and vertical temperatures by their respective currents. In a study focusing on the GFDL-ESM2M, Ng et al. (2014a) showed that nonlinear dynamic heating is conducive to IODE negative skewness by damping warm SSTAs but reinforcing cool SSTAs. However, given the uncertainty about the future change of nonlinear dynamic heating, greater model consensus is required to be confident about whether it will weaken or strengthen in the future (Cai et al. 2013).

Given the close proximity of aerosol-emitting regions such as eastern Asia and India to the Indian Ocean, it is necessary to understand how aerosols impact the mean-state conditions and ocean–atmosphere feedbacks critical for SST skewness in the IODE region. Anthropogenic aerosol species such as sulfate and black carbon have been shown to alter premonsoonal rainfall in these regions (e.g., Lau and Kim 2006; Meehl et al. 2008) and even impact tropical Pacific SSTs (Allen et al. 2014). If,

[1] The skewness is defined as $m_3(m_2)^{-3/2}$, where $m_k = \sum_{i=1}^{N}(x_i - \overline{X})^k/N$ is the kth moment and x_i is the ith model or observational value, $\overline{X}$ is the model or observational climatological mean, and N the length of the model or observational period (56 yr in this study).

TABLE 1. CMIP5 models used in this study. Also shown is the preindustrial control (piControl) experiment years used, and whether individual models include the first and second indirect aerosol effects.

Model	Modeling group	First indirect	piControl years (r1i1p1)	Reference
CanESM2	CCCma, Canada	Yes	2511–3010	von Salzen et al. (2013)
CCSM4	NCAR, United States	No	801–1300	Gent et al. (2011)
CSIRO Mk3.6.0	CSIRO and Queensland Climate Change Centre of Excellence (QCCCE), Australia	Yes*	1–500	Rotstayn et al. (2010)
FGOALS-g2	LASG Center for Earth System Science (CESS), China	Yes	401–900	Li et al. (2013)
GFDL CM3	NOAA/GFDL, United States	Yes	1–500	Donner et al. (2011)
GFDL-ESM2M	NOAA/GFDL, United States	No	1–500	Dunne et al. (2012)
GISS-E2-H	NASA GISS, United States	Yes*	1180–1419 and 2410–2649**	Miller et al. (2014)
GISS-E2-R	NASA GISS, United States	Yes*	4000–4499	Miller et al. (2014)
IPSL-CM5A-LR	IPSL, France	Yes	1850–2349	Dufresne et al. (2013)
NorESM1-M	Norwegian Climate Centre (NCC), Norway	Yes*	701–1200	Iversen et al. (2012)

* Denotes models that also contain the second indirect effect. The aerosols concentrations in the GISS models are prescribed and are not forced by emissions as in their p3xxx experiments (not included).

** Only 480 piControl years are used for GISS-E2-H, instead of 500 yr because of the unavailability of model data.

and how, aerosols influence SST skewness will be crucial for understanding future projections of IOD variability, given that GHG emissions will continue to increase in the future and global aerosols levels have peaked and will decrease (Klimont et al. 2013). Here, we use CMIP5 models with single-factor experiments that allow a direct comparison between GHGs and aerosols on their impact on IODE SST skewness. The models and analysis procedures are described in section 2, while the results pertaining to the skewness and its association with the mean conditions are shown in section 3. Sections 4 and 5 detail the feedbacks that contribute to the SST skewness, while section 6 summarizes the findings.

2. Data and methods

We use model experiments that contain all anthropogenic and natural forcings (histALL), and individual forcings experiments with historical anthropogenic aerosol forcing only (histAA) and historical GHGs only (histGHG). Table 1 lists the 10 models used in this study, and whether they include the first and second indirect aerosol effects (e.g., Wilcox et al. 2013). The direct effect refers to the scattering and absorption of radiation, while first and second indirect effects describe aerosol–cloud interactions (e.g., increased cloud droplet size, cloud lifetime). For each model we investigate their first experiment only [e.g., r1i1p*X*; see Taylor et al. (2012) for more information on the experiment notation and Collins et al. (2013) for aerosol species treated within individual models].

The mean anthropogenic conditions at all grid points are calculated for each model experiment, defined as the difference between the model's historical experiment (e.g., histGHG and histAA) and its 500-yr-long preindustrial control (piControl) experiment (see Table 1 for piControl years used[2]). This removes individual model biases that are unrelated to the anthropogenic forcings so a direct comparison between model mean conditions based purely on their individual responses to aerosols and GHGs can be made. The mean zonal gradients across the tropical Indian Ocean are defined as the average conditions over the IODW region minus the IODE region (i.e., moving eastward). As such, a positive (negative) mean zonal gradient in SST, thermocline, and precipitation means that the IODW region is warmer (cooler) and wetter (drier) than the IODE region.

To provide further differentiation of the role of aerosols and GHGs, four experiments from the CSIRO Mk3.6.0 model are examined. Five members make up each experiment type. These include histAA, histGHG, histALL, and an additional experiment that includes all forcings except for anthropogenic aerosols, which are held at preindustrial levels [called histNoAA; details are given in Rotstayn et al. (2012)]. By directly comparing histNoAA with histALL, we determine how the mean conditions and air–sea feedbacks are affected by excluding aerosols, as opposed to the experiments forced by only aerosols and GHGs.

All CMIP5 model outputs are bilinearly interpolated onto a $1° \times 1°$ grid with monthly data stratified into the mature IOD season (SON). While our intent is not to compare models with observations [refer to Cai and Qiu (2013) and Liu et al. (2014)], we initially compare model

[2] It should be noted that FGOALS-g2 piControl years are listed in Table 1; however, because of its unrealistic simulation of IODE SST skewness, the piControl years were not included in later analysis.

SST trends and skewness in the Indo-Pacific region with observations from the National Oceanic and Atmospheric Administration Extended Reconstructed SST version 3b (ERSST.v3b) dataset (Smith et al. 2008). A different observational product, called the Hadley Centre Global Sea Ice and Sea Surface Temperature dataset (Rayner et al. 2003), shows good agreement in terms of the Indo-Pacific SST skewness to ERSST.v3b (not shown); however, it suffers from erroneous cooling in the eastern equatorial Pacific Ocean during the twentieth century (Deser et al. 2010).

For the Bjerknes feedback responses, outputs of SST, thermocline depth at 20°C (Z20), and 850-mb wind are processed (1 mb = 1 hPa). Precipitation and evaporation fields are also assessed for their response to winds and SST. For the nonlinear dynamic heating feedback, outputs of zonal and meridional currents, and ocean temperature averaged over the top 50 m are processed, while the vertical transport is calculated via the continuity equation (Ng et al. 2014a). The dynamic and thermodynamic feedbacks are calculated through linear regression (e.g., Ng et al. 2014a; Liu et al. 2014; Cai and Qiu 2013; Russell and Gnanadesikan 2014), whereby anomalies of a given field (e.g., SST) averaged over a given region (e.g., IODE) are split into positive and negative samples; this represents the opposing conditions during positive and negative IOD events. All regressions are undertaken in the SON season, at each grid point for the positive and negative samples, so an assessment of the coupling asymmetry for each feedback response can be calculated. The coupling asymmetry is defined as the difference between the regression coefficient for positive and negative samples. The statistical significance for trends and regressions of the multimodel ensemble (MME) mean are determined using a two-sided Student's t test. For the spatial patterns highlighting the feedback asymmetries, we show significance at the 99% confidence level due to the high number of model years (56 yr for each model). For the areal-averaged feedback coupling asymmetries over a given region, individual experiment significance is based upon whether the 95% confidence limits for positive and negative coupling coefficients, used to calculate the asymmetry, overlap (asterisks in bar charts). To determine whether the difference between the aerosol- and GHG-forced asymmetries is significant, we calculate asymmetry values in each model's piControl experiment over 500 yr (based on a 56-yr sliding window). Error bars based on the one standard deviation of the piControl spread are attached to each anthropogenic-forced asymmetry, and where overlapping does not occur, the asymmetry difference between histAA and histGHG is considered to be statistically significant. Significance for each anthropogenic MME asymmetry value is based on the standard deviation of the coupling coefficients among the nine individual models (as FGOALS-g2 is excluded).

3. SST skewness and mean conditions

a. Indo-Pacific SST trends and skewness

Both the observed and simulated tropical Indo-Pacific SST trends over the twentieth and early twenty-first centuries (1900–2005) resemble a positive IOD-like pattern (cf. ERSST.v3b with the histALL MME in Figs. 1a,b). A zonal SST trend gradient (IODW minus IODE) is a feature of the tropical Indian Ocean, which is enhanced by GHGs driving a strong IODW warming (Fig. 1c). Over the 106-yr period the zonal SST trend gradient for the histGHG ensemble is 0.35°C, almost double that of the histALL gradient (0.19°C). Aerosols, on the other hand, enhance the cooling in the IODW region compared to the IODE, generating a distinctive negative IOD pattern (Fig. 1d) and a zonal SST trend gradient (−0.12°C). The negative IOD trend pattern is a robust feature induced by aerosols (Xie et al. 2013); however, the IODE region can exhibit a weak warming in CMIP5 models that only include the aerosol direct effect (Dong and Zhou 2014). Another feature is the aerosol-induced interhemispheric gradient in the cooling, which represents the spatially inhomogeneous distribution of aerosols, with more emissions from the Northern Hemisphere (e.g., Cai et al. 2006). The reduced warming (cooling) in the southeastern Pacific in the histGHG (histAA) MME is most likely in response to the wind–evaporation–SST feedback, whereby the southeast trades intensify (weaken) under the forcing of GHGs (aerosols) (Xie et al. 2013). This feedback describes how evaporation varies as a result of anomalous wind strength, leading to either a reinforcement or damping of SSTAs, depending on the season (Ng et al. 2014a).

We next compare the SST skewness between observations and MMEs in the Indo-Pacific basin over 1950–2005 (Fig. 2). The observations (ERSST.v3b) capture the negative SST skewness along the Sumatra–Java coast (Fig. 2a), which occurs only during SON (Hong et al. 2008a). As such, the strong positive skewness in the IOD predominantly arises because of SST IODE skewness (Ogata et al. 2013), as the IODE SST variance is larger than that in the IODW region (Hong et al. 2008c). Strong positive SST skewness is also a feature of the eastern tropical Pacific, because the amplitude of El Niño is larger than La Niña (Cai et al. 2012). Under all forcings (i.e., histALL), the MME average of 10 models broadly captures the observed SST skewness in the Indo-Pacific basin (Fig. 2b), despite showing a strong

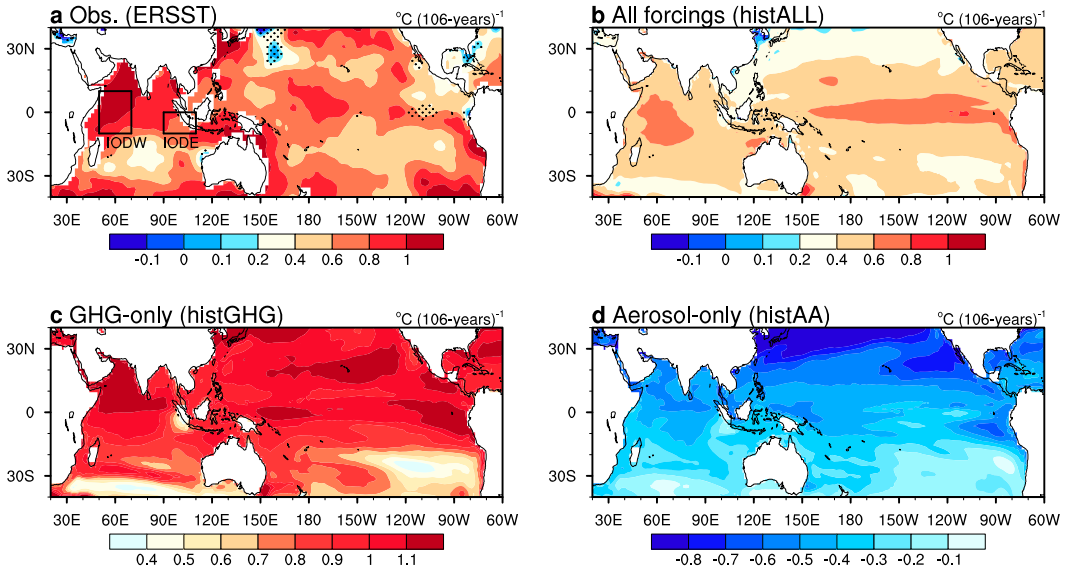

FIG. 1. Trend in SON SST in the tropical and subtropical Indo-Pacific Ocean for 1900–2005 from (a) observations (ERSST.v3b), and an MME mean of 10 models with (b) all forcings (histALL), (c) GHG-only forcing (histGHG), and (d) aerosol-only forcing (histAA). The MME consists of the first experiment from each model. Stippling in (a) covers trends that are not statistical significant at the 95% confidence level based on a *t* test. All MME trends are significant at the 95% confidence level and are therefore not stippled. Note that the color legends for (a),(b) are the same, whereas (c),(d) are different to highlight the zonal gradient across the equatorial Indian Ocean. The west and east poles of the IOD (IODW and IODE, respectively) are shown as rectangles in (a).

westward bias in IODE SST skewness. In the far western Pacific, close to the Philippine Sea, the simulated negative skewness is opposite to the observations; this bias is prominent in CMIP5 models such as CSIRO Mk3.6.0, GISS-E2-R, IPSL-CM5A-LR, and CCSM4 (Zhang and Sun 2014), and may be related to the warm pool extent (Sun et al. 2013).

The simulated skewness patterns in the histGHG and histAA MMEs are broadly similar (Figs. 2c and 2d, respectively) with both MMEs simulating a strong negative SST skewness in the IODE region and the westward bias. The skewness is more enhanced for histAA than for histGHG, confirmed by comparing each model's respective individual histAA and histGHG experiments (Fig. 2e). Six out of the 10 models (CanESM2, CSIRO Mk3.6.0, GISS-E2-H, GISS-E2-R, GFDL CM3, and CCSM4) have multiple experiments (≥3) to test whether the IODE SST skewness difference between anthropogenic experiments is robust. Eight out of the 10 models show an enhanced IODE SST skewness in their first histAA experiment. Only FGOALS-g2 and IPSL-CM5A-LR capture a stronger IODE SST skewness in their respective histGHG simulations. However, three out of five GISS-E2-H histAA experiments exhibit weaker skewnesses compared to the respective histGHG experiments. The FGOALS-g2 also simulates an unrealistically strong positive IODE SST skewness in both anthropogenic experiments. As such, this model is subsequently excluded from further analysis in this study (as in Ng et al. 2014b). Given that 23 out of 29 histAA experiments show a more enhanced IODE skewness than does histGHG, this provides confidence that the model results are not an artifact of choice of experiment. Thus, we focus on the possible reasons for the enhanced IODE SST skewness under an aerosol forcing. We first investigate the role that the tropical Indian Ocean mean state plays in contributing to the IODE SST skewness.

b. Indian Ocean mean conditions

A comparison is made between the mean anthropogenic SST, thermocline depth, precipitation, and 850-mb winds in experiments that include only aerosols (histAA) and GHGs (histGHG). The anthropogenic conditions are referred as GHG forced (i.e., histGHG minus piControl) and aerosol forced (histAA minus piControl). For the GHG- (aerosol-) forced surface conditions, the IODE (IODW) region exhibits a weaker (enhanced) warming (cooling) (Figs. 3a,b). These tropical Indian Ocean patterns represent a broad positive (negative) IOD-like mean state in response to GHGs (aerosols). The mean zonal gradients are more obvious for the thermoclines, with GHGs inducing a relatively weaker deepening in the IODE region compared to the

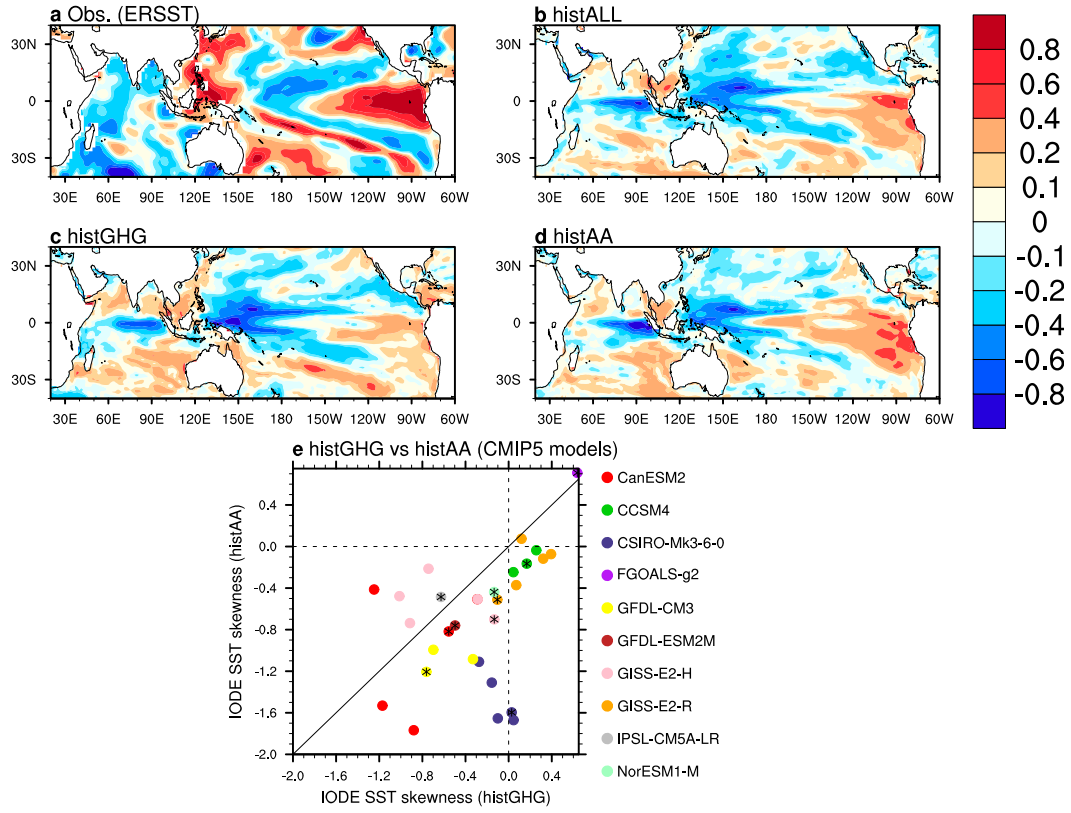

FIG. 2. Skewness in detrended SON SST in the tropical and subtropical Indo-Pacific Ocean for 1950–2005 from (a) observations (ERSST.v3b), and an MME with (b) histALL, (c) histGHG, and (d) histAA. (e) Comparison of IODE SST skewness for histAA (vertical axis) and histGHG (horizontal axis) experiments for the 10 CMIP5 models. Where available, multiple experiments are included, with the asterisks indicating the first experiment used for the MME regression analysis. Models below (above) the diagonal line indicate the IODE SST skewness is more enhanced in the histAA (histGHG) experiment.

IODW (Fig. 3c). For aerosols, a deepening is seen along the Sumatra–Java coast and a shoaling in the Arabian Sea (Fig. 3d). As such, a deeper (shallower) IODW thermocline relative to the IODE reflects a positive (negative) mean zonal thermocline gradient. The response to GHGs (aerosols) in the atmosphere reflects the underlying ocean conditions, with reduced (enhanced) precipitation associated with low-level easterlies (westerlies), predominantly east of 80°E (Figs. 3e and 3f, respectively). The mean conditions highlight the Bjerknes feedback response: in response to GHGs (aerosols), the mean zonal SST gradient along the equatorial Indian Ocean is positive (negative), coinciding with anomalous easterlies (westerlies) that suppress (enhance) convection in the IODE region. In response to the anomalous easterlies (westerlies), equatorial Kelvin waves uplift (deepen) the mean IODE thermocline, which then, in turn, determines the magnitude of the zonal SST gradient (Cai et al. 2013).

To test how the mean zonal gradients in SST, thermocline, precipitation, and zonal wind over the tropical Indian Ocean influence IODE SST skewness, based on an intermodel comparison, the first histALL, histGHG, and histAA experiment is used from the nine models. For SST, thermocline, and precipitation, we define the mean zonal gradient as IODW minus IODE [this is the definition of the dipole mode index, a measure of the IOD (Saji et al. 1999)]. As the zonal wind can be described as a response to SST gradients, we average the zonal wind over the eastern equatorial Indian Ocean (EEIO; 10°S–0°, 80°–100°E; see Fig. 3e for region), where the response is greatest (Cai and Cowan 2013). The intermodel comparison results suggest that the mean zonal gradients of SST, thermocline, and precipitation have a statistically significant (95% confidence level) association with IODE SST skewness (Figs. 4a–c, respectively). In response to aerosols, the mean zonal gradients tend to be negative across the Indian Ocean in all three parameters, with stronger negative gradients associated with enhanced IODE SST skewness. The GHG-forced thermoclines have a tendency to favor positive mean zonal gradients (i.e.,

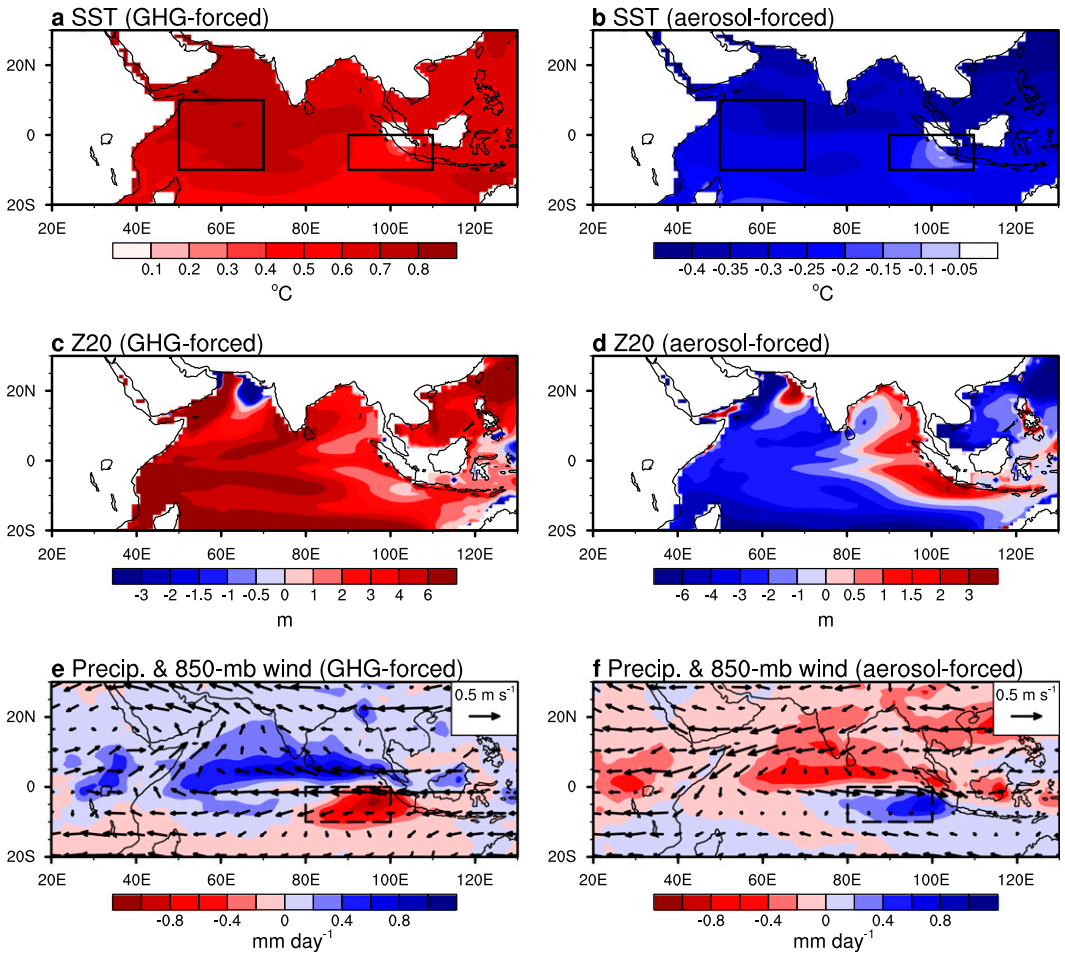

FIG. 3. Mean anthropogenic conditions in SON for 1950–2005 of (a),(b) SST, (c),(d) Z20, and (e),(f) precipitation (contours) and 850-mb wind (vectors), for (left) GHG-only and (right) aerosol-only MMEs (nine models, excluding FGOALS-g2). The anthropogenic conditions are calculated as the difference between each model's anthropogenic experiment (histGHG and histAA) and their 500-yr-long piControl experiment (see Table 1 for piControl years used). Note that the color legends in (a),(b) are different to highlight the zonal gradient. The IODW and IODE regions are shown with the rectangles in (a),(b) to highlight the zonal gradient across the equatorial Indian Ocean. In (e),(f) the EEIO region is shown with the dashed rectangle (10°S–0°, 80°–100°E).

positive IOD), with the histALL experiments showing a slight positive bias when compared to observations (Cai and Cowan 2013). This may reflect the fact that CMIP5 models either underestimate the response to an aerosol forcing (possibly as a result of the representation of the direct and indirect effect) or overestimate the response to GHGs. Under aerosols (GHGs), westerlies (easterlies) over the EEIO region are seen (Fig. 4d), consistent with the mean zonal gradients in precipitation and SST. For SST and thermocline, the mean zonal gradient–IODE SST skewness relationship is mostly controlled by the IODW conditions, and not locally (not shown). This implies that the mean IODE thermocline depth itself is less important in determining the magnitude of the IODE SST skewness from an intermodel perspective, but is controlled by the magnitude of the zonal gradient.

To provide further evidence of the mean zonal gradient's control on skewness, single-forcing experiments from the CSIRO Mk3.6.0 are analyzed, including histNoAA, to test the linearity of the interexperiment responses. We calculate the relationship between the mean zonal gradients and IODE SST skewness (Fig. 5), which can be directly compared to the intermodel relationship (Fig. 4). Comparing all four experiment types, the most obvious feature is the well-separated clusters of the histAA and histGHG (and histNoAA) members. Strong negative zonal gradients are seen in the aerosol-only experiments, as is enhanced negative SST skewness. The linear relationships between the mean zonal

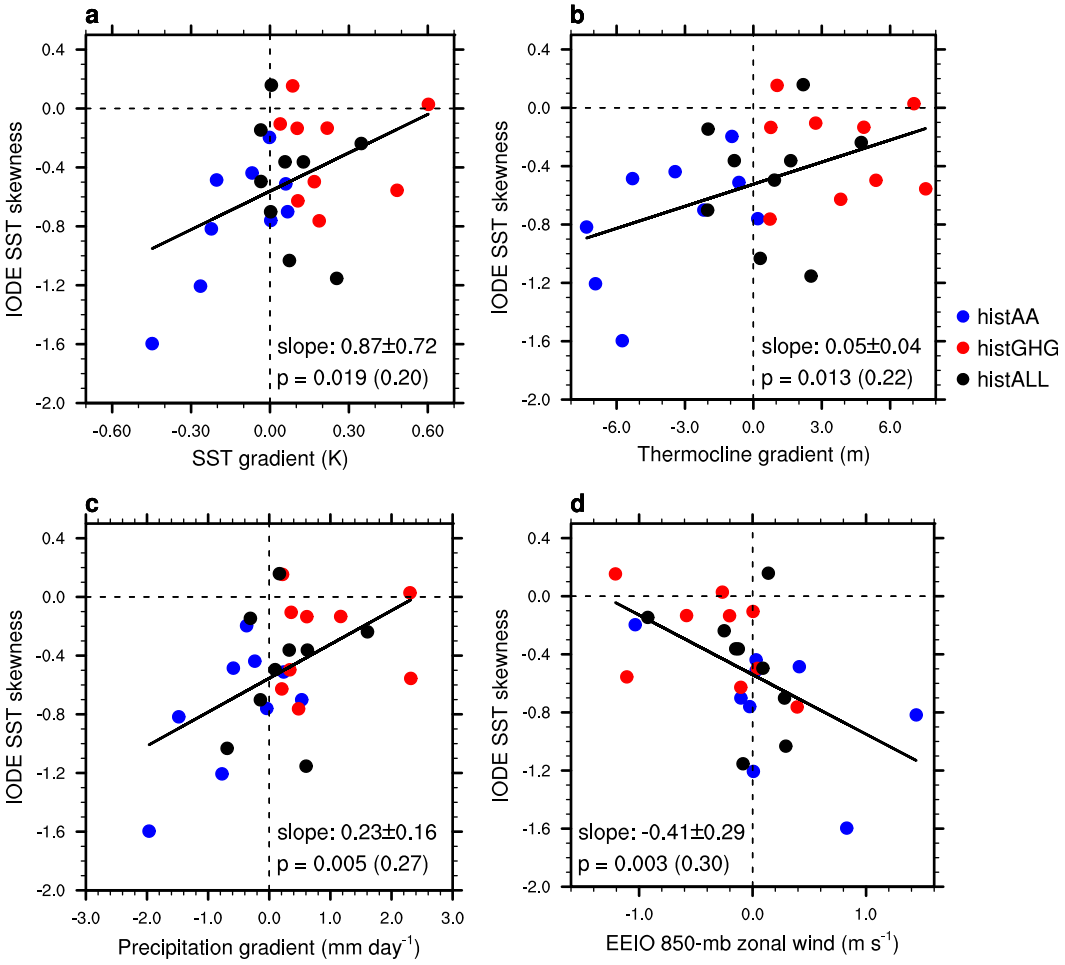

FIG. 4. Intermodel association between the detrended IODE SST skewness (vertical axis) and the mean zonal gradient (IODW minus IODE; horizontal axis) for (a) SST, (b) thermocline depth, and (c) precipitation, for the histAA, histGHG, and histALL experiments. (d) The 850-mb zonal wind over the EEIO is shown instead of zonal gradient. The unforced component, calculated from each model's 500-yr-long piControl experiment, is first removed from the respective historical experiment, averaged over 1950–2005. The regression slopes ±95% confidence intervals, p values, and R^2 values in parentheses for all samples are shown in each panel.

gradients (and EEIO zonal wind) with IODE SST skewness are statistically significant above the 99% confidence level, such that mean zonal gradients are directly proportional to the skewness magnitude. The clear distinction between histAA and histNoAA highlights the strong aerosol-induced skewness response in the CSIRO Mk3.6.0 associated with the slope of the mean zonal gradients.

Delving further into the mean conditions for this model again suggests that the IODW region is more important in controlling the mean zonal gradient–IODE SST skewness relationship than are the local IODE conditions (not shown). Both the intermodel and CSIRO Mk3.6.0 interexperiment results provide evidence that in response to aerosols (GHGs), IODW SSTs undergo an anomalous cooling (warming) associated with an anomalously shallow (deep) IODW thermocline. The response of IODE precipitation to zonal SST gradients, the associated response of EEIO zonal winds, and the ensuing thermocline gradients all confirm that the ocean–atmosphere mean state plays a key role in the IODE SST skewness. However, despite the statistically significant association between the zonal gradients with IODE SST skewness (Fig. 4), other factors, such as intermodel differences in monsoon intensity (Song et al. 2014), may also, in part, explain the intermodel mean state differences. The mean-state analysis does reveal that the coupling between the ocean and atmosphere is crucial. In the following section we investigate whether asymmetries in the air–sea feedbacks can provide an explanation as to why aerosols enhance the IODE SST skewness more so than for GHGs.

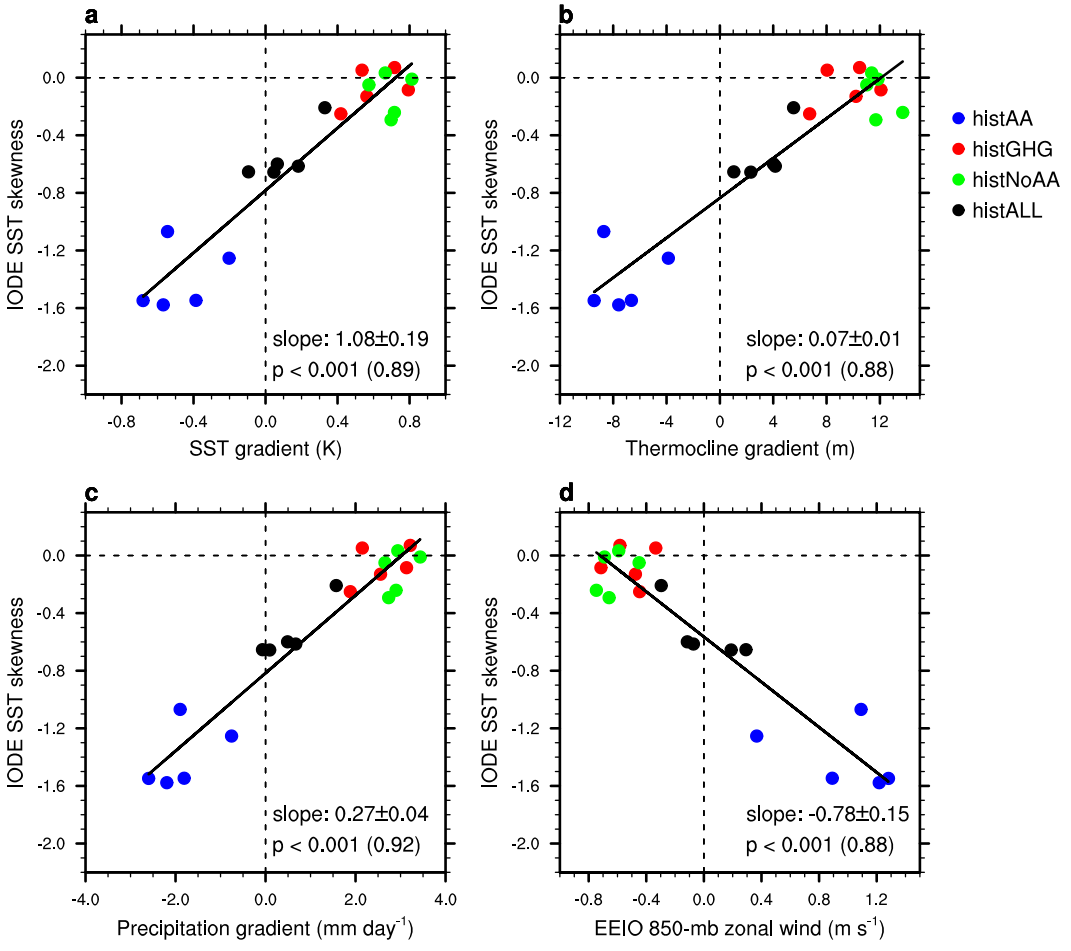

FIG. 5. The association between detrended IODE SST skewness (vertical axis) and mean zonal gradient (IODW minus IODE; horizontal axis) of (a) SST, (b) thermocline depth, and (c) precipitation, for histAA (blue), histGHG (red), histNoAA (green), and histALL (black) in CSIRO Mk3.6.0. (d)The 850-mb zonal wind over the EEIO is used instead of the zonal gradient. The unforced component, calculated from a 500-yr-long piControl experiment, is first removed from the respective historical experiments, averaged over 1950–2005. The regression slopes ±95% confidence intervals, p values, and R^2 values in parentheses are shown in each panel.

4. The role of the Bjerknes feedback

a. Asymmetry patterns

We first analyze the Bjerknes feedback, and then focus on the response of precipitation and evaporation to SSTAs and zonal winds. Before calculating the feedback asymmetries, we separate each parameter into positive and negative IODE samples (e.g., warm/cool SSTA, deep/shallow thermocline anomalies, and westerly/easterly anomalies) in the mature IOD season, SON. We initially focus on how the entire tropical Indian Ocean (i.e., predictand) responds linearly to changes, over 56 yr (1950–2005), in a given parameter over a particular region (i.e., predictor), and then focus on the IODE and IODW regions. We calculate the coupling (regression) coefficients at each grid point to show the relationship between the predictor and the predictand (as in Liu et al. 2011). Asymmetry patterns show the difference between the regression maps for positive and negative samples based on conditions over the IODE region (e.g., warm minus cool, deep minus shallow, and westerly minus easterly).

In all three experiments (histALL, histGHG, and histAA), the asymmetric SST response to thermocline anomalies (hereafter SST→Z20) is reproduced, meaning a shoaling thermocline induces a stronger surface cooling than a surface warming induced by a deepening thermocline. The area with such asymmetry stretches from Sumatra–Java to the western equatorial Indian Ocean (~30°E) (Fig. 6, left). In the histGHG MME, an asymmetry pattern exists across the South China Sea and off the northwest coast of Australia (Fig. 6d), as a result of a greater SST response to a deepening thermocline anomaly

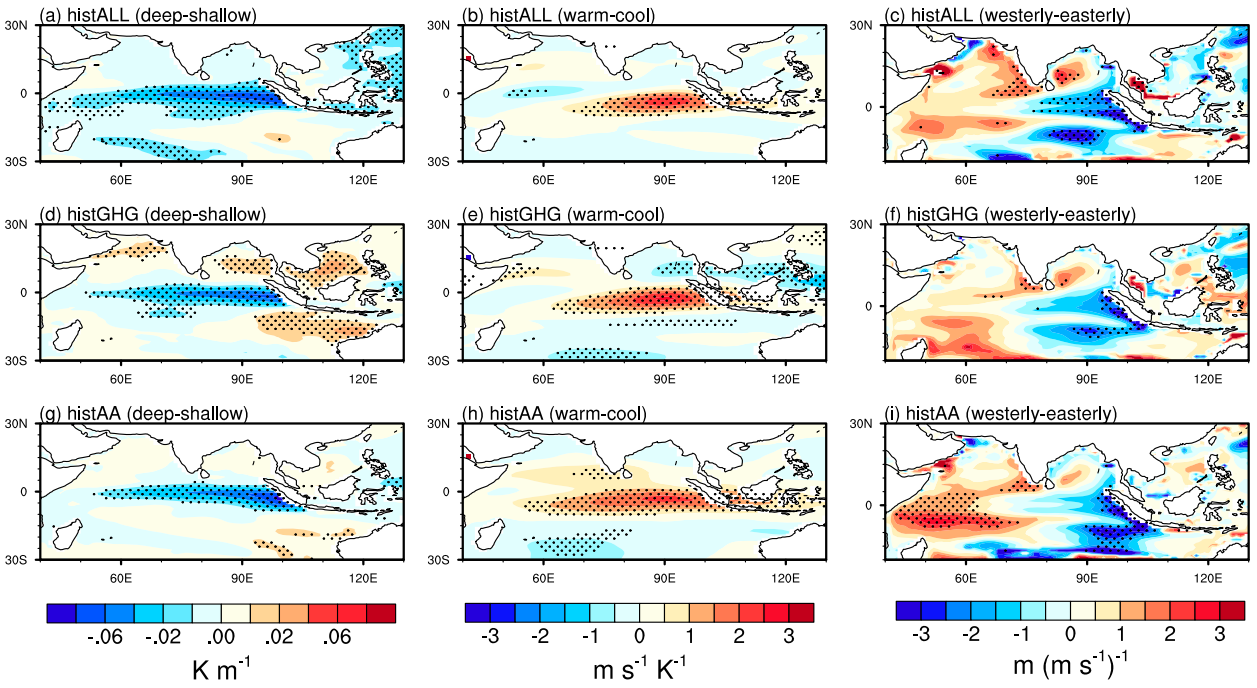

FIG. 6. Asymmetry in the Bjerknes feedback processes of (left) gridpoint SST to IODE thermocline depth ($K\,m^{-1}$), (center) gridpoint 850-mb zonal winds to IODE SSTA [$(m\,s^{-1})\,K^{-1}$], and (right) gridpoint thermocline to EEIO zonal wind anomalies [$m\,(m\,s^{-1})^{-1}$], for (a)–(c) histALL, (d)–(f) histGHG, and (g)–(i) histAA MMEs. Asymmetry is calculated as regression coefficients for positive samples (deep thermocline, warm SSTAs, and westerly winds) minus negative samples (shallow thermocline, cool SSTAs, and easterly winds) for 1950–2005. Stippling represents significant asymmetry based on the difference of two regression coefficients for positive and negative samples.

(not shown). Over these same areas, as well as the IODE region, the aerosol-induced surface response to an anomalously deep thermocline is far weaker than for GHGs.

As part of the Bjerknes feedback, the near-surface wind response to SSTAs (hereafter wind → SST) describes how zonal winds respond to a zonal SST gradient converging on regions of strong convection. In all MMEs there is a greater wind → SST response to warm IODE SSTAs simulated in the IODE region (Fig. 6, center). Little difference exists between the aerosol and GHG-induced wind→SST asymmetry patterns (Figs. 6e,h), aside from a marginally westward extension in the asymmetric response in the histAA MME. This asymmetry response is opposite to the observations, which show that the amplitudes of the wind anomalies during cool IODE SSTAs are much stronger than for warm IODE SSTAs (Hong et al. 2008a; Cai and Qiu 2013). Despite the tendency for CMIP5 models to underestimate this process (Liu et al. 2014), the wind→SST is not a major factor in contributing to the IODE SST skewness (Ng et al. 2014b), given the greater response during warm IODE SSTAs (i.e., unfavorable for negative skewness).

The thermocline response to zonal wind anomalies (hereafter Z20→wind) from the EEIO region closes the Bjerknes feedback loop. Here, an EEIO westerly (easterly) anomaly is associated with a deepening (shoaling) thermocline in the IODE region and vice versa for the IODW region. This generates an asymmetry in the IODE region favorable for SST skewness enhancement (Fig. 6, right). CMIP5 models tend to overestimate this response in the histALL experiments (Liu et al. 2014). This bias is seen in the histAA and histGHG MMEs, which capture a greater thermocline response to easterly wind anomalies along the Sumatra–Java coast. However, a stronger IODW thermocline response to easterly anomalies than to westerly anomalies is only simulated in the histAA MME. This represents a classic IOD pattern across the tropical Indian Ocean (Fig. 6i).

b. *SST response to thermocline*

To investigate the intermodel variations in the Bjerknes feedback asymmetry in the IODE region, individual model asymmetry coefficients for SST→Z20 (Fig. 7a), wind→SST (Fig. 7b), and Z20→wind (for both the IODE and IODW thermocline; Figs. 7c,d) are calculated (first experiment only). Individual model asymmetries are considered statistically significant if the 95% confidence intervals of the positive and negative

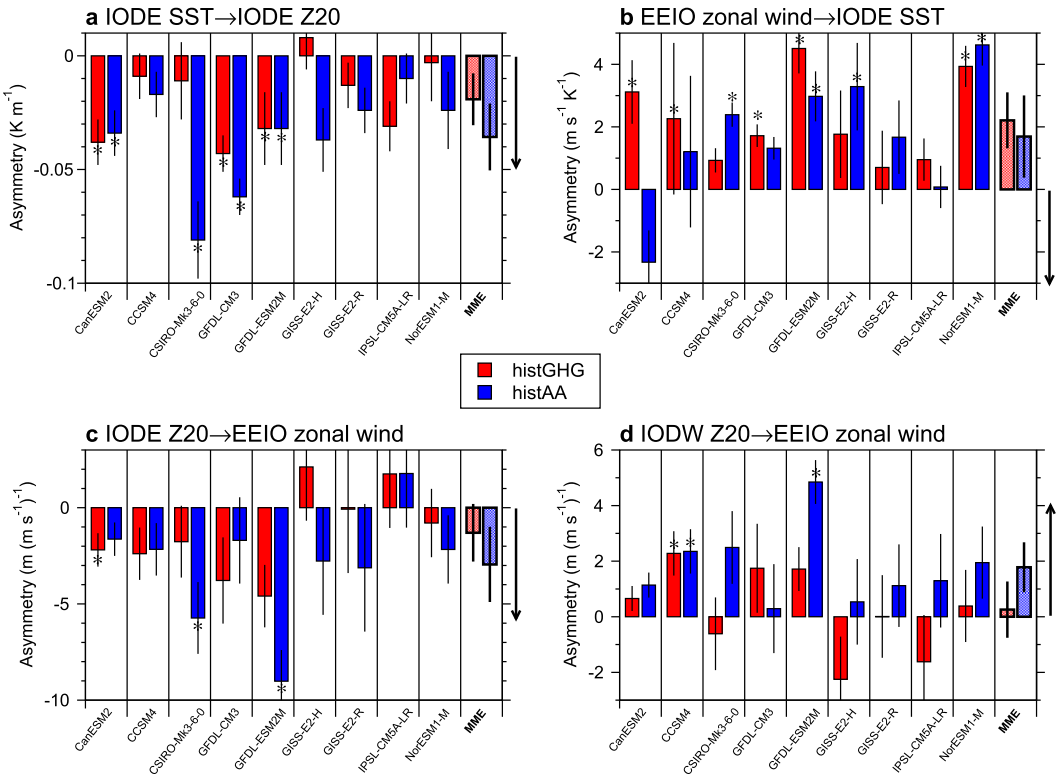

FIG. 7. Asymmetry in the Bjerknes feedback over the IODE region for histGHG (red) and histAA (blue) for individual models and MMEs. Asymmetry is defined as the difference in coupling coefficients between positive and negative samples. Shown are (a) IODE SST response to IODE thermocline anomalies (IODE SST→IODE Z20), (b) EEIO 850-mb zonal wind response to IODE SSTAs (EEIO wind→IODE SST), (c) IODE thermocline response to EEIO 850-mb zonal wind anomalies (IODE Z20→EEIO zonal wind), and (d) IODW thermocline response to EEIO 850-mb zonal wind anomalies (IODW Z20→EEIO zonal wind), calculated for 1950–2005. The asterisks indicate asymmetries where the 95% confidence intervals for the coupling coefficients do not overlap, considered statistically significant. Individual model error bars indicate the standard deviation of the feedback asymmetries calculated across 500 yr of the piControl experiment, using a 56-yr sliding window. The MME error bars represent the 95% confidence intervals based on the standard deviation among the nine model asymmetry values. Arrows on the right-hand side of each panel represent the asymmetry that would favor a negative SST skewness over the IODE region.

coupling coefficients do not overlap (as indicated by asterisks in Fig. 7). Also shown in Fig. 7 is the MME asymmetry coefficients and their 95% confidence interval based on the standard deviation of the asymmetries among the nine models, and whether the asymmetries favor negative IODE SST skewness (Fig. 7, arrows).

In nearly all models, the SSTA response to an anomalously shallow IODE thermocline is greater than for a deeper thermocline, thus generating asymmetry that favors negative IODE SST skewness (Fig. 7a). In quantifying the SST→Z20 asymmetry (deep minus shallow IODE thermocline), six out of the nine models display a stronger asymmetry in their histAA experiment than for histGHG, with GFDL-ESM2M and CanESM2 displaying almost equal asymmetry. For CSIRO Mk3.6.0, the SST→Z20 asymmetry in its histAA experiment is around 8 times larger than for its histGHG experiment. For the MMEs, the SST→Z20 responds to an anomalously shallow thermocline is very similar in magnitude between histAA and histGHG ($\sim$0.06 K m^{-1}), for aerosols (not shown). However, there is a weaker SST coupling when the thermocline is anomalously deep. The histAA MME asymmetry is almost double the histGHG asymmetry, although the difference between them is not quite statistically significant given the error bars overlap. The intermodel results from SST→Z20 reaffirm the importance of the mean zonal thermocline gradient across the tropical Indian Ocean (Fig. 4). During negative IOD events, further heating in the IODE region not only deepens the thermocline, but also enables its westward expansion, making the IODE SST→Z20 coupling weak. The opposite tilt of the GHG-induced mean zonal thermocline means that in

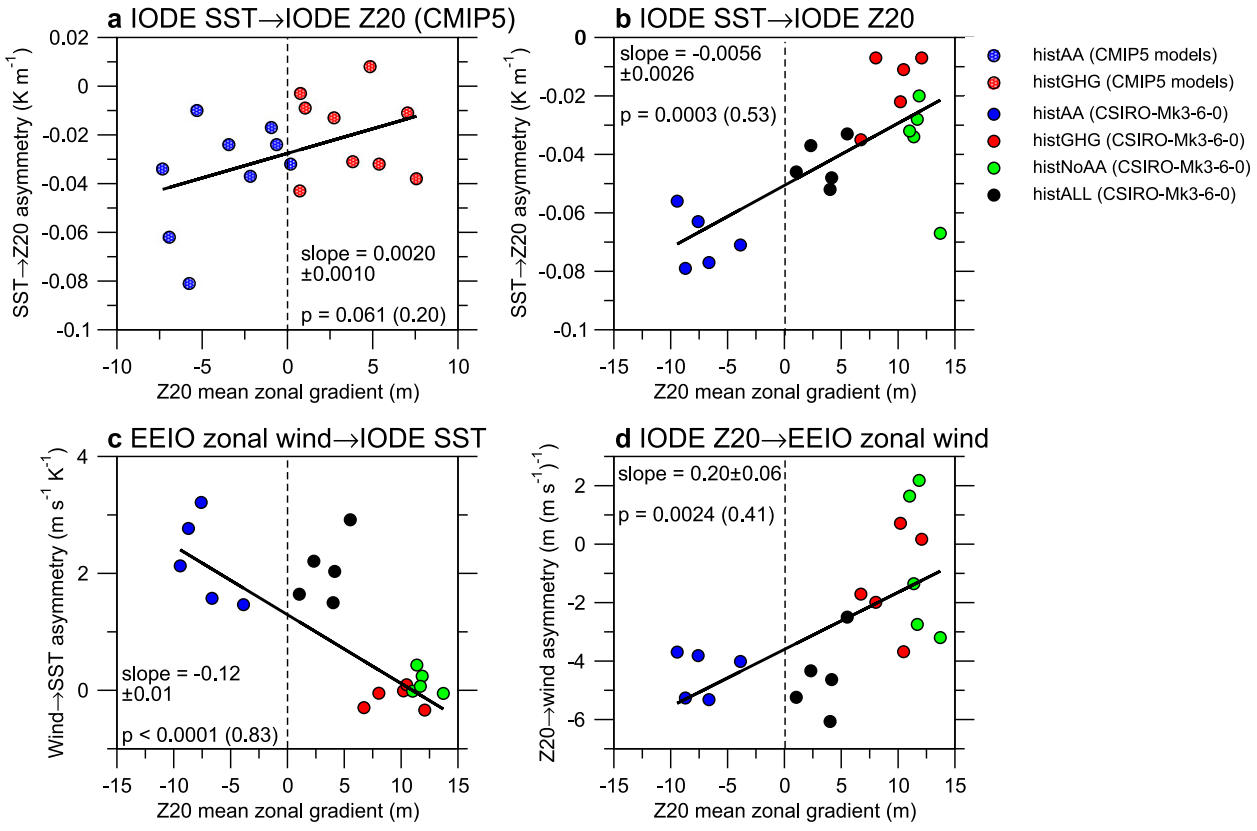

FIG. 8. The association between mean thermocline zonal gradient across the tropical Indian Ocean (horizontal axis) and asymmetry values (vertical axis) of (a) the IODE SST response to IODE thermocline anomalies (IODE SST→IODE Z20), for the nine CMIP5 models for histAA (blue-stippled circles) and histGHG (red-stippled circles). (b)–(d) The association between the mean thermocline zonal gradient across the tropical Indian Ocean (horizontal axis) and the Bjerknes feedback asymmetry values for CSIRO Mk3.6.0 (vertical axis), including (b) IODE SST→IODE Z20, (c) EEIO 850-mb zonal wind→IODE SST, and (d) IODE Z20→EEIO 850-mb zonal wind, for histAA (blue-filled circles), histGHG (red-filled circles), histNoAA (green-filled circles), and histALL (black-filled circles). The unforced component, calculated from a 500-yr-long piControl experiment, is first removed from the respective historical experiments, averaged over 1950–2005. The regression slopes ±95% confidence intervals, p values, and R^2 values in parentheses are shown in each panel.

the case of an anomalous deepening, the IODE thermocline is able to couple with SSTs, reducing the asymmetry.

Does the mean zonal thermocline gradient across the tropical Indian Ocean control the SST→Z20 asymmetry in the CMIP5 models? To determine this, we plot the SST→Z20 asymmetry against the mean zonal thermocline gradient from a CMIP5 intermodel perspective (Fig. 8a) and from a CSIRO Mk3.6.0 interexperiment perspective (Fig. 8b). It shows that the conditions induced by aerosols are such that the IODE thermocline is deeper relative to that in the IODW region. As such, IODE SSTs are only slightly perturbed when the thermocline deepens further during negative IOD events, thus creating the asymmetry. This relationship in the intermodel comparison is not as strong as for CSIRO Mk3.6.0, perhaps reflecting disparities in how each model responds to aerosol forcings [i.e., the exclusion of the indirect aerosol effect (Dong and Zhou 2014)] and/or internal model forcings. Given the internal forcings in CSIRO Mk3.6.0 are the same between different experiments, they exhibit stronger clustering (Fig. 8b). For CSIRO Mk3.6.0, without an aerosol forcing (i.e., histNoAA) the mean IODE thermocline shoals to a depth such that the SST→Z20 response to further thermocline perturbations is less asymmetric between warm and cool IODE phases (Fig. 8b).

c. *Wind response to SST*

The EEIO zonal wind→IODE SSTA (Fig. 7b) does not reflect the asymmetric response in SST→Z20. As in the spatial patterns (Fig. 6, center), the zonal wind along the eastern equatorial Indian Ocean is strongly coupled to warm SSTAs and only weakly coupled to cool SSTAs, an asymmetry unfavorable for enhancing negative SST skewness. Only CanESM2 shows a stronger zonal wind

response to cool IODE SSTAs in its histAA experiment (opposite asymmetry value in Fig. 7b), which possibly reinforces the negative SST skewness in the EEIO region in this model (not shown); however, the asymmetry is not statistically significant. Given the individual model asymmetries for wind→SST are opposite to what one would expect to enhance negative SST skewness, this component of the Bjerknes feedback is not a factor in the skewness differences between histGHG and histAA. In fact, the wind→SST is more representative of the SST–cloud–radiation feedback (Ng et al. 2014a). Under cloudless conditions the response of the zonal winds to cool IODE SSTAs is small. Warm IODE SSTAs, on the other hand, promote convection and enhance precipitation, allowing the zonal winds to strengthen. This results in the strong wind response to warm IODE SSTAs.

Further analysis reveals a lack of an intermodel relationship between the mean zonal SST gradient and the asymmetric wind→SST response, although a relationship exists in the CSIRO Mk3.6.0 experiments, both in the mean zonal gradients of SST (not shown) and the thermocline (Fig. 8c). An aerosol-induced mean zonal thermocline gradient is associated with a strong asymmetric wind→SST; however, the asymmetry is almost identical in the histALL experiments (Fig. 8c, black dots). This suggests that wind→SST is capped at a zonal thermocline gradient threshold. Increasing the tilt of the mean thermocline across the Indian Ocean (i.e., deeper in the east under an aerosol forcing) appears not to further enhance the wind→SST asymmetry, even though the asymmetry plays no role in the generating the negative SST skewness.

d. Thermocline response to wind

The Z20→wind asymmetry over the IODE and IODW regions is shown in Figs. 7c and 7d, respectively. Most models exhibit a more typical Bjerknes feedback response over the IODE region, such that the thermocline responds more strongly to EEIO easterly anomalies than to westerlies, consistent with SST→Z20 asymmetry response. For the IODE region, the thermocline uplift induced by easterly anomalies is greater than the deepening forced by a similar strength of westerly anomalies, as shown in recent observations (Cai and Qiu 2013). The Z20→wind asymmetry also favors a negative IODE SST skewness (Fig. 7c, arrow). Of the models, only GFDL-ESM2M and CSIRO Mk3.6.0 display both significant aerosol-induced asymmetries in their SST→Z20 and Z20→wind (Figs. 7a,c), even though most models show a greater asymmetry in their histAA experiment compared to histGHG.

The IODW thermocline, northeast of Madagascar, also responds to the low-level EEIO wind forcing, with anomalous easterlies (westerlies) driving an anomalous deepening (shoaling) that generates asymmetry (Fig. 6, right). The histGHG MME response in the IODW region is virtually symmetric to the different EEIO wind phases (Fig. 7d), even though the mean IODW thermocline is deeper (under GHGs), which is a common model bias (Cai and Cowan 2013). The histAA MME exhibits a strong asymmetry, reflecting the weak (strong) IODW thermocline response to anomalous westerlies (easterlies) in most models. The CSIRO Mk3.6.0 interexperiment relationship between the mean zonal thermocline gradient and Z20→wind asymmetry response is similar to the wind→SST response. Aerosols induce a tilt of the thermocline across the tropical Indian Ocean that does not proportionally increase the magnitude of the Z20→wind asymmetry response (Fig. 8d). However, in excluding aerosols (histNoAA), the mean thermocline tilts upward toward the east (west is deeper). This weakens the Z20→wind asymmetry as the thermocline is shallow enough to respond equally to both wind phases. This underscores the importance of aerosols forcing a shoaling thermocline in the western Indian Ocean, compared to the east, such that an anomalously deeper IODE thermocline is further isolated from the surface, relative to the west. Despite this, warm IODE SSTAs are able to generate a greater wind response, even though this process is unfavorable for negative SST skewness.

5. Other feedback processes

a. Precipitation response

We next focus on the response of precipitation to IODE SSTAs (hereafter precipitation→SST), as part of SST–cloud–radiation negative feedback loop. In model simulations it appears that the coupling between precipitation and the warm SSTAs over the IODE region is much stronger than for the cool SSTAs, generating significant asymmetry (Fig. 9, left; red colors), as seen in an ocean reanalysis (Hong and Li 2010). However, along the equator, the coupling between precipitation and the cool IODE SSTAs dominates the asymmetry, which extends westward into the IODW region (Fig. 9, left; blue colors). Both asymmetry patterns in the equatorial and off-equatorial Indian Ocean appear to be greater in magnitude in the histGHG experiments compared to histAA.

To investigate this further, we average the precipitation→SST coupling coefficients over two sectors. These are region 1, the equatorial eastern Indian Ocean (equator, 80°–100°E), and region 2, the off-equatorial eastern Indian Ocean (5°–10°S, 90°–110°E). For region 1, the precipitation→SST is highly nonlinear,

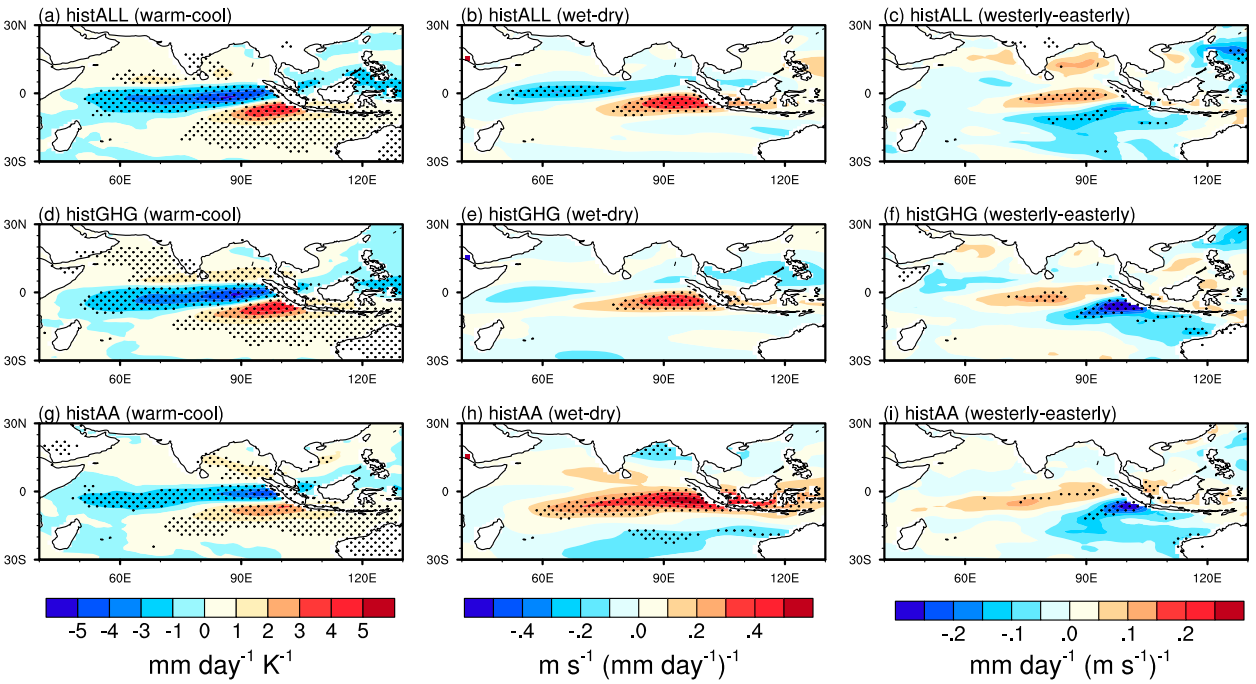

FIG. 9. Asymmetry response of (left) gridpoint precipitation to IODE thermocline depth [(mm day^{-1}) K^{-1}], (center) gridpoint 850-mb zonal winds to IODE precipitation [m s^{-1} (mm day^{-1})$^{-1}$], and (right) gridpoint evaporation to IODE 850-mb zonal wind anomalies [m s^{-1} (mm day^{-1})$^{-1}$], for (a)–(c) histALL, (d)–(f) histGHG, and (g)–(i) histAA MMEs. Asymmetry is calculated as regression coefficients for positive samples (warm SSTAs, anomalously wet, and westerly winds) minus negative samples (cool SSTAs, anomalously dry, and easterly winds). Stippling represents significant asymmetry based on the difference of two regression coefficients for positive and negative samples.

as with the observations (Cai and Qiu 2013), with stronger damping for cool IODE SSTAs than for warm SSTAs in both MMEs, generating asymmetries that do not support the negative SST skewness (Fig. 10a). The region 1 asymmetry difference between the histGHG and histAA MMEs arises because of the greater GHG-induced damping for cool IODE SSTAs, as the precipitation damping of warm IODE SSTAs is identical for both (not shown). For region 2, the MME response in both histGHG and histAA is opposite to that along region 1, with the damping significantly greater for warm IODE SSTAs than for cool SSTAs, creating an asymmetry response that enhances the IODE negative SST skewness (Fig. 10b). However, for region 2, the precipitation→SST asymmetry may partly cause IODE SST skewness through damping warm SSTAs more so than cool SSTAs. Given the difference between the histAA and histGHG MME asymmetries is not statistically significant, this feedback is unlikely to contribute to the enhanced aerosol-induced SST skewness.

It is necessary to understand the different asymmetric precipitation responses to IODE SSTAs along the equator, compared to the off-equatorial IODE region. During positive IOD events (i.e., cool IODE SSTAs), a band of atmospheric subsidence extends westward along the equator, resulting in low precipitation anomalies over both regions 1 and 2 (Cai et al. 2014); this process occurs in the majority of models (not shown). During negative IODs (i.e., warm IODE SSTAs), the convection contracts eastward to the IODE region. Thus, the off-equatorial Indian Ocean (region 2) experiences enhanced convection and precipitation, while the opposite occurs in equatorial region 1. This has been observed as the second orthogonal mode of extreme positive IOD events whereby suppressed convection in the IODE region shifts northward, and a band of the associated subsidence extends along the central equatorial Indian Ocean (Cai et al. 2014).

The zonal wind response to IODE precipitation (wind→precipitation) is almost identical to the wind→SST (Fig. 6, center), which displays an asymmetry extending out westward along the EEIO region. This infers that the EEIO zonal wind response to anomalously wet conditions (negative IOD) in the IODE region is stronger compared to anomalously dry conditions (positive IOD). This is confirmed by analyzing the individual model asymmetries (Fig. 10c). This helps explain the breakdown in the Bjerknes feedback with respect to the wind→SST. That happens because positive precipitation anomalies are indicative of

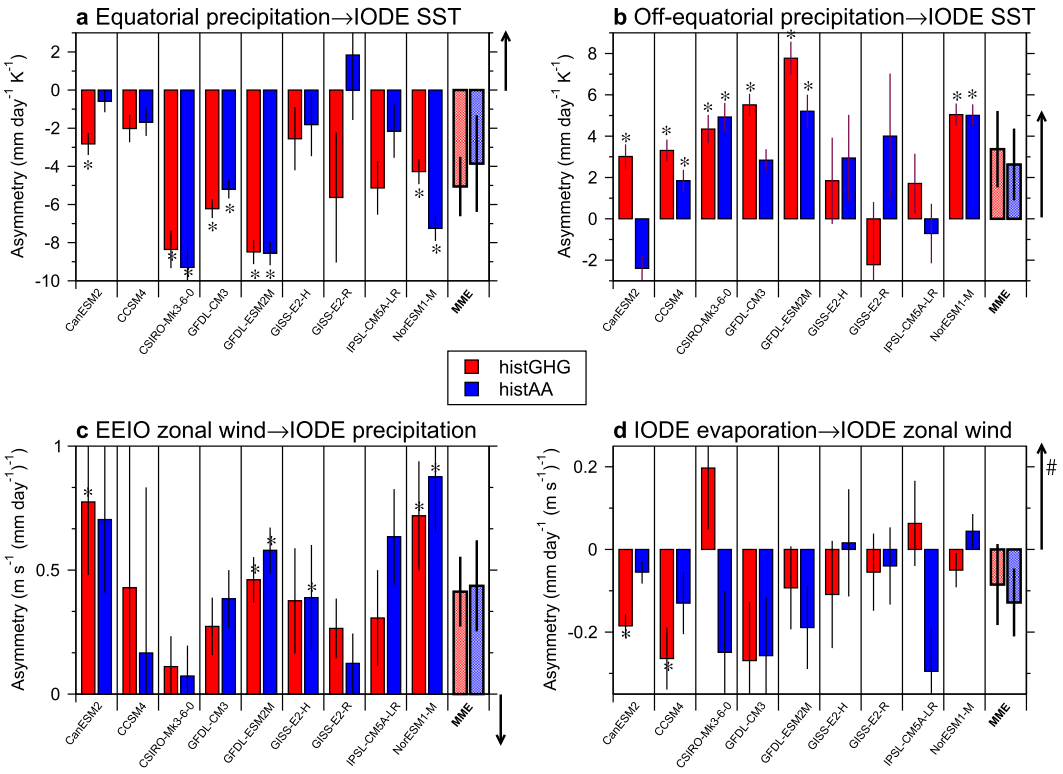

FIG. 10. Asymmetry response of precipitation, averaged (a) along the equator of the eastern Indian Ocean (equator, 80°–100°E) and (b) over the off-equatorial eastern Indian Ocean (5°–10°S, 90°–110°E), to IODE SSTA for histGHG (red) and histAA (blue) for nine models. (c) The response of EEIO 850-mb wind to IODE precipitation anomalies (EEIO zonal wind → IODE precipitation). (d) The response of IODE evaporation to IODE 850-mb zonal wind anomalies (IODE evaporation → IODE zonal wind). Asymmetry is defined as the difference in coupling coefficients between positive and negative samples, calculated for 1950–2005. The asterisks indicate asymmetries where the 95% confidence intervals for the coupling coefficients do not overlap, considered statistically significant. Individual model error bars indicate the standard deviation of the feedback asymmetries calculated across 500 yr of the piControl experiment, using a 56-yr sliding window. The MME error bars represent the 95% confidence intervals based on the standard deviation among the nine model asymmetry values. Arrows on the right-hand side of each panel represent the asymmetry that would favor a negative SST skewness over the IODE region. The number symbol (#) to the right of (d) refers to the fact that the evaporation → zonal wind asymmetry only favors skewness if the evaporation increases for stronger easterlies and cooler SSTAs, more so than for westerlies and warm SSTAs.

enhanced convection and a strong zonal pressure gradient, associated with an amplified EEIO westerly wind response. During cloudless conditions, there is a collapse of the SST–precipitation relationship, such that the zonal pressure gradient and coupling to EEIO easterly winds weakens. However, this process acts to weaken the negative IODE SST skewness (as with the wind → SST), implying that the zonal wind response does not cause SST skewness, but that the SST skewness occurs despite the atmospheric response.

b. Evaporation response

The evaporation response to IODE wind anomalies (hereafter evaporation → wind), and evaporation response to IODE SSTAs (hereafter evaporation → SST) show a similar pattern of asymmetry across the tropical Indian Ocean (we only show the evaporation → wind response in Fig. 9, right column). Over the IODE region the asymmetric response is such that evaporation is reduced more during a positive IOD event (easterly wind anomalies, cool SSTAs) than it is enhanced during a negative IOD (westerly wind anomalies and warm SSTAs). This occurs despite the weaker wind → SST during positive IOD conditions, confirming that evaporation is more responsive to SSTAs than to the zonal wind speed (Ng et al. 2014a). There is a wide diversity in evaporation → wind asymmetries (for the IODE region) across the individual models (Fig. 10d), with the MMEs of both histGHG and histAA showing only small insignificant differences. Given this, and the fact that the evaporation response to IODE SST and wind feedbacks are negative, the IODE negative SST skewness is

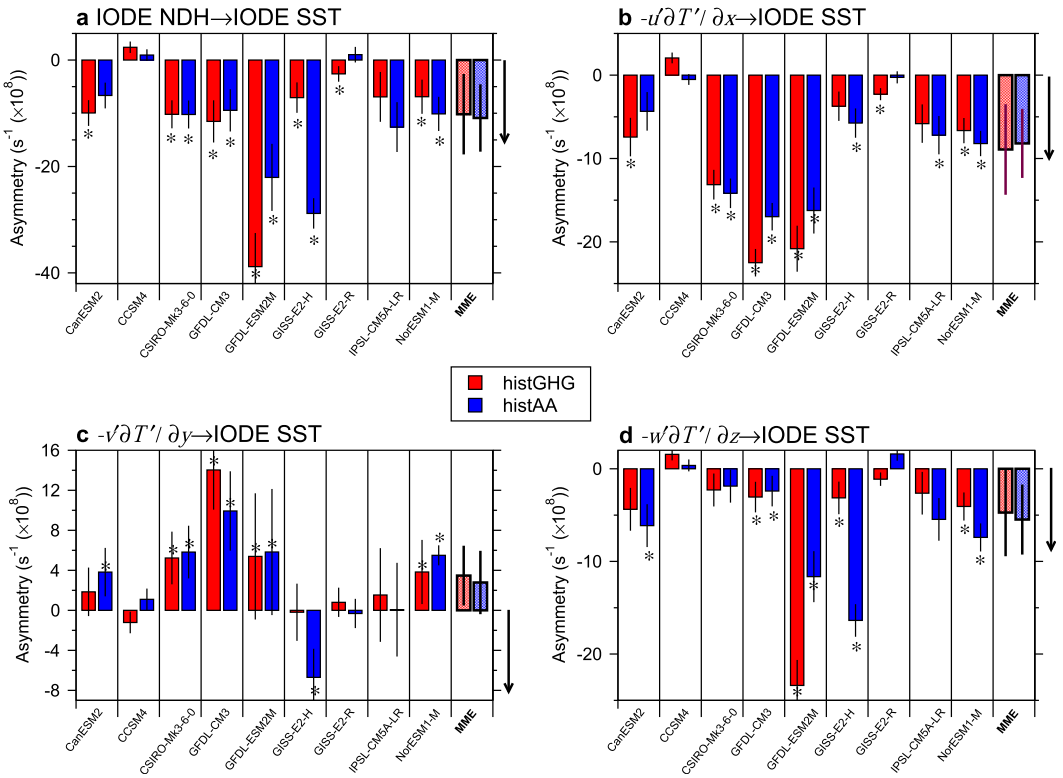

FIG. 11. Asymmetry response ($10^8\,s^{-1}$) of (a) IODE nonlinear dynamic heating, (b) IODE anomalous zonal advection of temperature ($u'\partial T'/\partial x$), (c) IODE anomalous meridional advection of temperature ($v'\partial T'/\partial y$), and (d) IODE anomalous vertical advection of temperature ($w'\partial T'/\partial z$), to the IODE SSTA for histGHG (red) and histAA (blue) for nine models. Asymmetry is defined as the difference in coupling coefficients between positive and negative samples, calculated for 1950–2005. The asterisks indicate asymmetries where the 95% confidence intervals for the coupling coefficients do not overlap, considered to be statistically significant. Individual model error bars indicate the standard deviation of the feedback asymmetries calculated across 145 yr (1861–2005) of the histALL experiment, using a 56-yr sliding window (due to the unavailability of the piControl experiment for nonlinear dynamic heating). The MME error bars represent the 95% confidence intervals based on the standard deviation among the nine model asymmetry values. Arrows on the right-hand side of each panel represent the asymmetry that would favor a negative SST skewness over the IODE region.

generated in the models, despite the response of evaporation to SSTAs and winds.

c. *Nonlinear dynamic heating*

The last feedback covered is the response of nonlinear dynamic heating to SSTAs (hereafter nonlinear dynamic heating → SST). To test whether significant asymmetry differences occur between aerosol- and GHG-forced experiments, individual temperature advection asymmetries to IODE SSTAs are calculated (Fig. 11). The results for individual models suggest that GHGs, in general, cause a strong nonlinear dynamic heating damping of warm IODE SSTAs, more so than reinforcing cool SSTAs (not shown), generating strong asymmetry in models like GFDL-ESM2M and GFDL CM3. However, across the models the asymmetry is similar under an aerosol forcing, given that the damping effect is weaker for warm SSTAs, but the reinforcing influence is stronger (than for histGHG) for cool SSTAs events. As such, the MME asymmetry difference between GHGs and aerosols is negligible (Fig. 11a). The asymmetry in the total nonlinear dynamic heating merely reflects the nonlinear zonal and vertical temperature advection terms (Figs. 11b,d), with aerosols (GHGs) strongly reinforcing (damping) cool (warm) SSTAs, contributing to the negative IODE SST skewness. The meridional temperature advection response to IODE SSTAs is similar in the aerosol and GHG MMEs with both more strongly damping cool IODE SSTAs, and reinforcing warm SSTAs, generating near-equal asymmetries (Fig. 11c). Across all three temperature advection components, only GISS-E2-H displays significant asymmetries in its histAA experiments, which may partly explain why it simulates more enhanced

TABLE 2. Summary of the anthropogenic forcing experiment that simulates an IODE feedback process that exhibits the largest asymmetry favoring negative SST skewness. The processes shown are 1) IODE SST→IODE Z20 (Fig. 7a), 2) IODE Z20→EEIO wind (Fig. 7c), 3) off-equatorial precipitation→IODE SST (Fig. 10b), 4) IODE nonlinear dynamic heating→IODE SST (Fig. 11a), 5) zonal temperature advection→IODE SST (Fig. 11b), and 6) vertical temperature advection→IODE SST (Fig. 11d). The asymmetry values are based on the difference in coupling coefficients between positive and negative IODE samples, calculated over 1950–2005. The tilde refers to equal asymmetry between histGHG and histAA. Significant asymmetries are in boldface. The models are listed in order from strongest to weakest IODE SST skewness in histAA (i.e., CSIRO Mk3.6.0 exhibits the largest skewness). The experiments in italics represent asymmetries that are significantly different from their respective anthropogenic counterpart. Anthropogenic aerosols are abbreviated AA.

Model	1	2	3	4	5	6
CSIRO Mk3.6.0	***AA***	***AA***	**AA***	∼**	**AA***	GHG
GFDL CM3	***AA****	GHG	***GHG***	**GHG***	***GHG****	**GHG***
CanESM2	**GHG***	***GHG***	***GHG***	**GHG**	**GHG**	**AA**
GFDL-ESM2M	∼**	**AA**	***GHG****	***GHG****	**GHG***	***GHG****
GISS-E2-H	*AA*	AA	AA	***AA****	**AA**	***AA****
GISS-E2-R	AA	AA	*AA*	***GHG***	***GHG***	*AA*
IPSL-CM5A-LR	GHG	∼	GHG	AA	**AA**	AA
NorESM1-M	AA	AA	∼**	**AA***	**AA***	***AA****
CCSM4	AA	∼	***GHG****	GHG	*GHG*	GHG
MME	AA	AA	GHG	∼	∼	∼

* Refers to other experiment also capturing significant asymmetry, but with a smaller magnitude.
** Both equally significant asymmetries.

IODE negative SST skewness. However, while nonlinear dynamic heating strongly favors negative SST skewness in the IODE region, the negligible differences between the GHG- and aerosol-induced asymmetric responses in the MMEs implies that this feedback cannot account for the enhanced SST skewness in the IODE region seen in the histAA experiments. As aerosols continue to decrease in the future, the nonlinear dynamic heating effect that reinforces cool IODE SSTAs should weaken, while the damping of warm SSTAs will increase as a result of increasing GHGs, as projected in GFDL-ESM2M (Ng et al. 2014a).

6. Discussion and conclusions

In this study, we investigated why cool SSTAs near Sumatra–Java can grow larger than warm SSTAs (negative skewness), and why anthropogenic aerosols enhance this asymmetry more so than GHGs. Our two-step aim was to first understand the role of mean anthropogenic conditions in enhancing the SST skewness and, second, whether the asymmetric responses in ocean–atmosphere feedbacks were important. For this we used CMIP5 model experiments that included only anthropogenic aerosols (i.e., histAA) and GHGs (i.e., histGHG). Previous research has suggested that the IODE SST skewness arises because of the deep mean thermocline in the IODE region, such that when the thermocline shoals, it is more effective in generating a surface cooling than it can induce a warming following a thermocline deepening (Zheng et al. 2010; Cai et al. 2013). Our results suggest that, in fact, the sign and magnitude of the mean zonal thermocline gradient across the tropical Indian Ocean are important factors. The west–east tilt of the mean zonal thermocline and SST is controlled by the anthropogenic forcing in question, with aerosols (GHGs) generating a negative (positive) gradient. A negative (positive) mean zonal thermocline gradient reflects a greater deepening (shoaling) in the IODE region, relative to the IODW, and is more strongly (weakly) associated with IODE SST skewness. Precipitation across the tropical Indian Ocean responds accordingly to these zonal ocean gradients, showing a strong relationship to IODE SST skewness through its association with the mean local winds, which in turn act upon the thermocline.

In establishing the importance of mean zonal gradients in determining the magnitude of the IODE SST skewness, focus then shifted to the dynamic and thermodynamic feedbacks and their asymmetric responses. A summary of each feedback process that favors negative IODE SST skewness (Bjerknes, precipitation–SST, and nonlinear dynamic heating feedbacks), as to whether the asymmetric response is greater in histAA or histGHG for each model, is listed in Table 2 (models are ranked from largest aerosol-induced negative IODE SST skewness to smallest).[3] The importance of the SST→Z20 in generating the enhanced SST skewness for aerosols is obvious, with six out of nine models

[3] The wind–evaporation–SST feedback, and wind→SST and wind→precipitation are excluded as they do not favor negative skewness.

generating a greater SST→Z20 asymmetry in their histAA experiment than in histGHG. The asymmetry in the SST→Z20 process reflects the weak SST response to a deepening thermocline, which is weaker again in the histAA experiment. This asymmetric response is somewhat proportional to the mean zonal thermocline gradient from an intermodel perspective, but highly significant from an interexperiment perspective from CSIRO Mk3.6.0, such that the more negative the mean zonal thermocline gradient (i.e., deeper IODE thermocline than for IODW), the stronger the SST→Z20 asymmetry. When the thermocline gradient is positive (i.e., GHG forced; IODE shallow, IODW deep), the thermocline is relatively less isolated from the surface in the IODE region, meaning the SST response to an anomalous deepening is slightly stronger.

The wind→SST asymmetry is opposite to the SST→Z20, in that winds in the central Indian Ocean are more strongly coupled to warm SSTAs, consistent with wind response to positive precipitation anomalies. The Z20→wind is consistent with the positive sign of the Bjerknes feedback, given that the thermocline deepens less in response to westerly anomalies than it uplifts when forced by easterly anomalies. For the other feedbacks, while some favor negative IODE SST skewness (e.g., nonlinear dynamic heating feedback and IODE precipitation response to IODE SSTAs), the fact that little difference is seen between the asymmetric response for GHGs and aerosols suggests that these processes cannot solely explain the aerosol-induced enhancement.

Understanding the intermodel comparison results is complicated by the many assumptions and limitations in the climate models. For example, not every model uses the same aerosol emission inventory (Wilcox et al. 2013) or includes an indirect aerosol forcing (Jones et al. 2013), shown to be important for offsetting the long-term Indian Ocean warming trends (Dong and Zhou 2014). In fact, a subset of four CMIP5 models that only includes the direct effect of aerosols generates a noticeable annual surface warming in the IODE region over the twentieth century, in contrast to a cooling in the western basin (Dong and Zhou 2014). This brings into question the impact of the direct aerosol effect on the Bjerknes feedback. Ideally, a comparison between direct versus indirect aerosol effects in the same model is worth investigating, now given the emergence of new targeted modeling experiments designed for this purpose. Many CMIP5 models also contain biases associated with the Bjerknes feedback, including weaker coupling strengths between the ocean and atmosphere, weak IOD amplitudes, and overly deep thermoclines (Liu et al. 2014). Some models also favor a particular IOD state, as shown for the CMIP3 model, FGOALS-g1 (Dong et al. 2014). Uncertainty also lies with the interaction between aerosols and clouds, and how they are parameterized in the models (Sherwood et al. 2013). Convection parameterization schemes can alter where the mean convection and prevailing winds are located (Russell and Gnanadesikan 2014), potentially impacting air–sea feedbacks. What this study has shown is that the separation of processes impacted by GHGs and aerosols is far clearer in an individual model (e.g., CSIRO Mk3.6.0), rather than solely relying on a MME framework approach, given the broad range of model responses to anthropogenic forcings (e.g., Jones et al. 2013). This is the first step in delineating the major external factors that enhance IODE SST skewness in the CMIP5 models and will help us to understand what a future response may be as aerosols decline and GHGs continue to increase.

Acknowledgments. This research is supported by the Australian Climate Change Science Program and the ARC Centre of Excellence in Climate System Science. Part of this research was undertaken on the NCI National Facility in Canberra, Australia, which is supported by the Australian Commonwealth Government. We acknowledge the World Climate Research Programme's Working Group on Coupled Modelling for CMIP5. Finally, we thank Arnold Sullivan and three anonymous reviewers for helpful comments to the manuscript.

REFERENCES

Allen, R. J., J. R. Norris, and M. Kovilakam, 2014: Influence of anthropogenic aerosols and the Pacific decadal oscillation on tropical belt width. *Nat. Geosci.,* **7,** 270–274, doi:10.1038/ngeo2091.

Behera, S. K., J.-J. Luo, S. Masson, P. Delecluse, S. Gualdi, A. Navarra, and T. Yamagata, 2005: Paramount impact of the Indian Ocean dipole on the East African short rains: A CGCM study. *J. Climate,* **18,** 4514–4530, doi:10.1175/JCLI3541.1.

Cai, W., and T. Cowan, 2013: Why is the amplitude of the Indian Ocean dipole overly large in CMIP3 and CMIP5 climate models? *Geophys. Res. Lett.,* **40,** 1200–1205, doi:10.1002/grl.50208.

——, and Y. Qiu, 2013: An observation-based assessment of nonlinear feedback processes associated with the Indian Ocean dipole. *J. Climate,* **26,** 2880–2890, doi:10.1175/JCLI-D-12-00483.1.

——, D. Bi, J. Church, T. Cowan, M. Dix, and L. Rotstayn, 2006: Pan-oceanic response to increasing anthropogenic aerosols: Impacts on the Southern Hemisphere oceanic circulation. *Geophys. Res. Lett.,* **33,** L21707, doi:10.1029/2006GL027513.

——, T. Cowan, M. Dix, L. Rotstayn, J. Ribbe, G. Shi, and S. Wijffels, 2007: Anthropogenic aerosol forcing and the structure of temperature trends in the southern Indian Ocean. *Geophys. Res. Lett.,* **34,** L14611, doi:10.1029/2007GL030380.

——, P. van Rensch, T. Cowan, and H. H. Hendon, 2012: An asymmetry in the IOD and ENSO teleconnection pathway and its impact on Australian climate. *J. Climate,* **25,** 6318–6329, doi:10.1175/JCLI-D-11-00501.1.

——, X.-T. Zheng, E. Weller, M. Collins, T. Cowan, M. Lengaigne, W. Yu, and T. Yamagata, 2013: Projected response of the Indian Ocean dipole to greenhouse warming. *Nat. Geosci.,* **6,** 999–1007, doi:10.1038/ngeo2009.

——, A. Santoso, G. Wang, E. Weller, L. Wu, K. Ashok, Y. Masumoto, and T. Yamagata, 2014: Increased frequency of extreme Indian Ocean dipole events due to greenhouse warming. *Nature,* **510,** 254–258, doi:10.1038/nature13327.

Collins, M., and Coauthors, 2013: Long-term climate change: Projections, commitments and irreversibility. *Climate Change 2013: The Physical Science Basis,* T. F. Stocker et al., Eds., Cambridge University Press, 1029–1136.

Cowan, T., W. Cai, A. Purich, L. Rotstayn, and M. H. England, 2013: Forcing of anthropogenic aerosols on temperature trends of the sub-thermocline southern Indian Ocean. *Sci. Rep.,* **3,** 2245, doi:10.1038/srep02245.

Deser, C., A. S. Phillips, and M. A. Alexander, 2010: Twentieth century tropical sea surface temperature trends revisited. *Geophys. Res. Lett.,* **37,** L10701, doi:10.1029/2010GL043321.

Dong, L., and T. Zhou, 2014: The Indian Ocean sea surface temperature warming simulated by CMIP5 models during the twentieth century: Competing forcing roles of GHGs and anthropogenic aerosols. *J. Climate,* **27,** 3348–3362, doi:10.1175/JCLI-D-13-00396.1.

——, ——, and B. Wu, 2014: Indian Ocean warming during 1958–2004 simulated by a climate system model and its mechanism. *Climate Dyn.,* **42,** 203–217, doi:10.1007/s00382-013-1722-z.

Donner, L. J., and Coauthors, 2011: The dynamical core, physical parameterizations, and basic simulation characteristics of the atmospheric component AM3 of the GFDL global coupled model CM3. *J. Climate,* **24,** 3484–3519, doi:10.1175/2011JCLI3955.1.

Dufresne, J.-L., and Coauthors, 2013: Climate change projections using the IPSL-CM5 earth system model: From CMIP3 to CMIP5. *Climate Dyn.,* **40,** 2123–2165, doi:10.1007/s00382-012-1636-1.

Dunne, J. P., and Coauthors, 2012: GFDL's ESM2 global coupled climate–carbon earth system models. Part I: Physical formulation and baseline simulation characteristics. *J. Climate,* **25,** 6646–6665, doi:10.1175/JCLI-D-11-00560.1.

Gent, P. R., and Coauthors, 2011: The Community Climate System Model version 4. *J. Climate,* **24,** 4973–4991, doi:10.1175/2011JCLI4083.1.

Hong, C.-C., and T. Li, 2010: Independence of SST skewness from thermocline feedback in the eastern equatorial Indian Ocean. *Geophys. Res. Lett.,* **37,** L11702, doi:10.1029/2010GL043380.

——, ——, L. Ho, and J.-S. Kug, 2008a: Asymmetry of the Indian Ocean dipole. Part I: Observational analysis. *J. Climate,* **21,** 4834–4848, doi:10.1175/2008JCLI2222.1.

——, ——, and J.-J. Luo, 2008b: Asymmetry of the Indian Ocean dipole. Part II: Model diagnosis. *J. Climate,* **21,** 4849–4858, doi:10.1175/2008JCLI2223.1.

——, M.-M. Lu, and M. Kanamitsu, 2008c: Temporal and spatial characteristics of positive and negative Indian Ocean dipole with and without ENSO. *J. Geophys. Res.,* **113,** D08107, doi:10.1029/2007JD009151.

Iversen, T., and Coauthors, 2012: The Norwegian Earth System Model, NorESM1-M—Part 2: Climate response and scenario projections. *Geosci. Model Dev. Discuss.,* **5,** 2933–2998, doi:10.5194/gmdd-5-2933-2012.

Jones, G. S., P. A. Stott, and N. Christidis, 2013: Attribution of observed historical near-surface temperature variations to anthropogenic and natural causes using CMIP5 simulations. *J. Geophys. Res. Atmos.,* **118,** 4001–4024, doi:10.1002/jgrd.50239.

Klimont, Z., S. J. Smith, and J. Cofala, 2013: The last decade of global anthropogenic sulfur dioxide: 2000–2011 emissions. *Environ. Res. Lett.,* **8,** 014003, doi:10.1088/1748-9326/8/1/014003.

Lau, K. M., and K. M. Kim, 2006: Observational relationships between aerosol and Asian monsoon rainfall, and circulation. *Geophys. Res. Lett.,* **33,** L21810, doi:10.1029/2006GL027546.

Li, L., and Coauthors, 2013: The flexible global ocean-atmosphere-land system model, grid-point version 2: FGOALS-g2. *Adv. Atmos. Sci.,* **30,** 543, doi:10.1007/s00376-012-2140-6.

Liu, L., W. Yu, and T. Li, 2011: Dynamic and thermodynamic air–sea coupling associated with the Indian Ocean dipole diagnosed from 23 WCRP CMIP3 models. *J. Climate,* **24,** 4941–4958, doi:10.1175/2011JCLI4041.1.

——, S.-P. Xie, X.-T. Zheng, T. Li, Y. Du, G. Huang, and W.-D. Yu, 2014: Indian Ocean variability in the CMIP5 multi-model ensemble: The zonal dipole mode. *Climate Dyn.,* **43,** 1715–1730, doi:10.1007/s00382-013-2000-9.

Meehl, G. A., J. M. Arblaster, and W. D. Collins, 2008: Effects of black carbon aerosols on the Indian monsoon. *J. Climate,* **21,** 2869–2882, doi:10.1175/2007JCLI1777.1.

Miller, R. L., and Coauthors, 2014: CMIP5 historical simulations (1850–2012) with GISS ModelE2. *J. Adv. Model. Earth Syst.,* **6,** 441–477, doi:10.1002/2013MS000266.

Ng, B., W. Cai, and K. Walsh, 2014a: Nonlinear feedbacks associated with the Indian Ocean dipole and their response to global warming in the GFDL–ESM2M coupled climate model. *J. Climate,* **27,** 3904–3919, doi:10.1175/JCLI-D-13-00527.1.

——, ——, and ——, 2014b: The role of the SST–thermocline relationship in Indian Ocean Dipole skewness and its response to global warming. *Sci. Rep.,* **4,** 6034, doi:10.1038/srep06034.

Ogata, T., S.-P. Xie, J. Lan, and X.-T. Zheng, 2013: Importance of ocean dynamics for the skewness of the Indian Ocean dipole mode. *J. Climate,* **26,** 2145–2159, doi:10.1175/JCLI-D-11-00615.1.

Rayner, N. A., D. E. Parker, E. B. Horton, C. K. Folland, L. V. Alexander, D. P. Rowell, E. C. Kent, and A. Kaplan, 2003: Global analyses of sea surface temperature, sea ice, and night marine air temperature since the late nineteenth century. *J. Geophys. Res.,* **108,** 4407, doi:10.1029/2002JD002670.

Rotstayn, L. D., M. A. Collier, M. R. Dix, Y. Feng, H. B. Gordon, S. P. O'Farrell, I. N. Smith, and J. Syktus, 2010: Improved simulation of Australian climate and ENSO-related rainfall variability in a global climate model with an interactive aerosol treatment. *Int. J. Climatol.,* **30,** 1067–1088, doi:10.1002/joc.1952.

——, S. J. Jeffrey, M. A. Collier, S. M. Dravitzki, A. C. Hirst, J. I. Syktus, and K. K. Wong, 2012: Aerosol- and greenhouse gas-induced changes in summer rainfall and circulation in the Australasian region: A study using single-forcing climate simulations. *Atmos. Chem. Phys.,* **12,** 6377–6404, doi:10.5194/acp-12-6377-2012.

——, M. A. Collier, S. J. Jeffrey, J. Kidston, J. I. Syktus, and K. K. Wong, 2013: Anthropogenic effects on the subtropical jet in the Southern Hemisphere: Aerosols versus long-lived greenhouse gases. *Environ. Res. Lett.,* **8,** 014030, doi:10.1088/1748-9326/8/1/0140302.

Russell, A. M., and A. Gnanadesikan, 2014: Understanding multidecadal variability in ENSO amplitude. *J. Climate,* **27,** 4037–4051, doi:10.1175/JCLI-D-13-00147.1.

Saji, N. H., B. N. Goswami, P. N. Vinayachandran, and T. Yamagata, 1999: A dipole mode in the tropical Indian Ocean. *Nature,* **401,** 360–363.

Sherwood, S. C., M. J. Alexander, A. R. Brown, N. A. McFarlane, E. P. Gerber, G. Feingold, A. A. Scaife, and W. W. Grabowski, 2013: Climate processes: Clouds, aerosols and dynamics. *Climate Science for Serving Society,* G. R. Asrar and J. W. Hurrell, Eds., Springer, 73–103, doi:10.1007/978-94-007-6692-1_4.

Smith, T. M., R. W. Reynolds, T. C. Peterson, and J. Lawrimore, 2008: Improvements to NOAA's historical merged land–ocean surface temperature analysis (1880–2006). *J. Climate,* **21,** 2283–2296, doi:10.1175/2007JCLI2100.1.

Song, F., T. Zhou, and Y. Qian, 2014: Responses of East Asian summer monsoon to natural and anthropogenic forcings in the 17 latest CMIP5 models. *Geophys. Res. Lett.,* **41,** 596–603, doi:10.1002/2013GL058705.

Sun, Y., D. Z. Sun, L. X. Wu, and F. Wang, 2013: Western Pacific warm pool and ENSO asymmetry in CMIP3 models. *Adv. Atmos. Sci.,* **30,** 940–953, doi:10.1007/s00376-012-2161-1.

Taylor, K. E., R. J. Stouffer, and G. A. Meehl, 2012: An overview of CMIP5 and the experiment design. *Bull. Amer. Meteor. Soc.,* **93,** 485–498, doi:10.1175/BAMS-D-11-00094.1.

Ummenhofer, C. C., M. H. England, P. C. McIntosh, G. A. Meyers, M. J. Pook, J. S. Risbey, A. S. Gupta, and A. S. Taschetto, 2009: What causes southeast Australia's worst droughts? *Geophys. Res. Lett.,* **36,** L04706, doi:10.1029/2008GL036801.

von Salzen, K., and Coauthors, 2013: The Canadian fourth generation Atmospheric Global Climate Model (CanAM4). Part I: Representation of physical processes. *Atmos.–Ocean,* **51,** 104–125, doi:10.1080/07055900.2012.755610.

Wilcox, L. J., E. J. Highwood, and N. J. Dunstone, 2013: The influence of anthropogenic aerosol on multi-decadal variations of historical global climate. *Environ. Res. Lett.,* **8,** 024033, doi:10.1088/1748-9326/8/2/024033.

Xie, S. P., B. Lu, and B. Q. Xiang, 2013: Similar spatial patterns of climate responses to aerosol and greenhouse gas changes. *Nat. Geosci.,* **6,** 828–832, doi:10.1038/ngeo1931.

Yadav, R. K., 2013: Emerging role of the Indian Ocean on Indian northeast monsoon. *Climate Dyn.,* **41,** 105–116, doi:10.1007/s00382-012-1637-0.

Zhang, T., and D.-Z. Sun, 2014: ENSO asymmetry in CMIP5 models. *J. Climate,* **27,** 4070–4093, doi:10.1175/JCLI-D-13-00454.1.

Zheng, X.-T., S.-P. Xie, G. A. Vecchi, Q. Liu, and J. Hafner, 2010: Indian Ocean dipole response to global warming: Analysis of ocean–atmospheric feedbacks in a coupled model. *J. Climate,* **23,** 1240–1253, doi:10.1175/2009JCLI3326.1.

——, ——, Y. Du, L. Liu, G. Huang, and Q. Liu, 2013: Indian Ocean dipole response to global warming in the CMIP5 multimodel ensemble. *J. Climate,* **26,** 6067–6080, doi:10.1175/JCLI-D-12-00638.1.